ORIGINAL PAPER

Molecular orbital evaluation of charge flow dynamics in natural pigments based photosensitizers

Thekinneydath Rajan Heera · Louis Cindrella

Abstract The relationship between structure and photo electrochemical property of ten natural pigments from plants, insects and microbes has been analyzed using density functional theory (DFT) at the B3LYP/6-31G(d) level. The essential parameters for their photoelectrochemical behaviour such as ground state geometries, electronic transition energies and oxidation potentials are computed. The attachment tendency of the anchoring groups, expressed as the deprotonation order, is determined by calculating the proton affinities at different sites of the molecules. A thorough analysis of the charge flow dynamics in the molecular orbitals (HOMO and LUMO) of these molecules has been carried out and presented to emphasize the role of these orbitals in effective charge separation, the important feature of photosensitizers for DSSC. This study highlights that the flexible spatial orientation provided by the bridging aliphatic unsaturation favours the oscillator strength and the hydroxyl anchor group attached to the ring of delocalized π electron cloud acts as the effective anchor.

Introduction

Solar electricity is the dependable clean energy of the future. Dye-sensitized solar cell (DSSC), based on porous nanocrystalline TiO$_2$ is considered as low-cost and high efficiency solar electricity system [1, 2]. The favourable

light absorption by photosensitizer and the charge-carrier transport to the semiconductor are separated in DSSCs. A potential photosensitizer for DSSC has to absorb all radiations in the visible region along with that of the UV and IR ranges of wavelength also. This has thrust focus on the identification of efficient dye to harvest a larger region of the solar spectrum [3]. In addition, it must attach to the semiconductor oxide surface and upon excitation it should inject electrons into the solid with a quantum yield of unity [4]. Also, the energy level of the excited state should be well matched to the lower bound of the conduction band of the oxide to minimize energetic losses during the electron transfer reaction. Its redox potential should be sufficiently high that it can be regenerated *via* electron donation from the redox electrolyte or the hole conductor. All these essential properties of a photosensitizer are structure-based and several natural dyes possess such favourable photo properties. Hence in order to correlate between the structure and photoelectrochemical properties, the theoretical analysis of ten naturally available dyes is carried out in this study to infer on the structure-implied coupling between the highest occupied molecular orbital (HOMO) and lowest unoccupied molecular orbital (LUMO), ground state geometry, HOMO and LUMO potentials, deprotonation order and charge flow dynamics. The time-dependent density functional theory (TD-DFT) developed by Runge and Gross [5] has become a widely used *ab initio* tool for theoretically evaluating excited state energies and more recently excited state geometries [6] and hence we have employed the same in this study.

Dyes from natural sources

Naturally available dyes have been successfully used in the textile industries. There are many dyes with fastness to

T. R. Heera · L. Cindrella (✉)
Department of Chemistry, National Institute of Technology,
Tiruchirappalli 620015, India
e-mail: cind@nitt.edu

sunlight and durability. Dyes obtained from natural products have been used as photosensitizers with acceptable efficiency. Several reports [7–12] have emphasized the use of natural extracts as a cheaper, faster, low-energy requiring and environmental friendly alternative for use in dye-sensitized solar cells [13–21]. Natural pigments from plants such as chlorophyll [13], carotenoids [8] and anthocyanins [8–10] have been extensively studied as photosensitizers for the DSSC. Hence motivated by the wide spread applications of natural pigments, this study has been undertaken to theoretically evaluate some of the unexplored natural pigments as photosensitizers for their possible application in DSSC. A choice of ten dyes from assorted sources such as plants, insects and microbes has been made.

They are caffeic acid, ferulic acid, ellagic acid, deoxysantalin, resveratrol (plant source), carminic acid, kersemic acid, ommatin D (insects), methoxatin and caulerpinic acid (microbes). Their structural formulae are given in Fig. 1.

Computational methods

The optimization of geometries of the singlet ground state of the above ten natural pigments was carried out using DFT [22, 23] calculations with B3LYP/6-31G (d) [24] basis set. DFT method has been chosen in this study due to the fact that the geometry optimizations are faster than that by the MP methods [25]. The choice of B3LYP functional was

a

(E)-3-(3,4-dihydroxyphenyl)acrylic acid

(Caffeic acid)

4-hydroxy-3-methoxy cinnamic acid
(Ferulic acid)

2,3,7,8-tetrahydroxychromeno[5,4,3-cde]chromene-5,10-dione
(Ellagic acid)

b

6-acetyl-2,5,7,8-tetrahydroxy-4-methyl-9,10-dioxo-9,10-dihydroanthracene-1-carboxylic acid
(Kermesic acid)

3,5,6,8-tetrahydroxy-1-methyl-9,10-dioxo-7-(2,3,4-trihydroxy-5-(hydroxymethyl)cyclohexyl)-9,10-dihydroanthracene-2-carboxylic acid
(Carminic acid)

4,5-dioxo-4,5-dihydro-1H-pyrrolo[2,3-f]quinoline-2,7,9-tricarboxylic acid
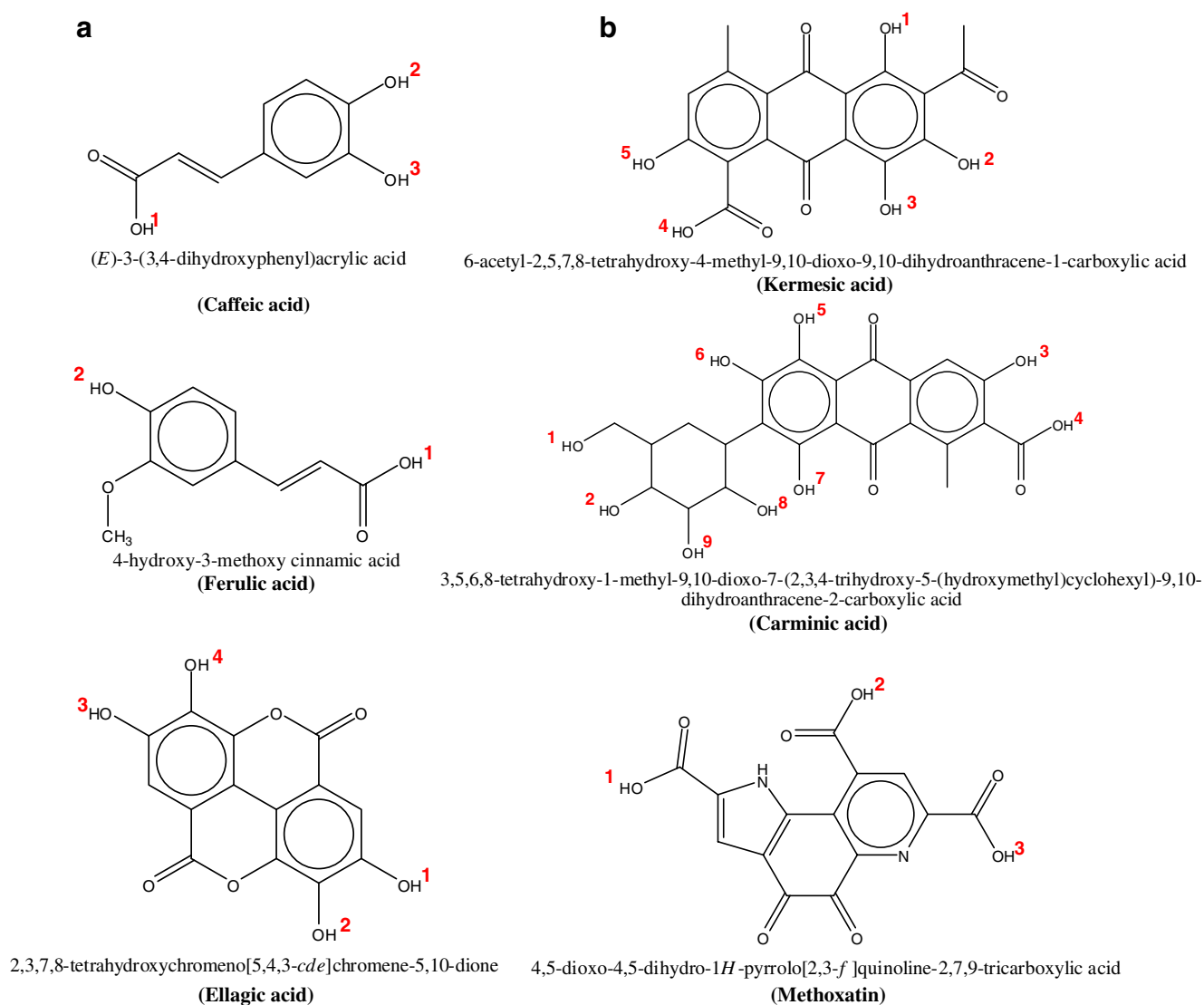**(Methoxatin)**

Fig. 1 **a** Structure of caffeic acid, ferulic acid and ellagic acid with their sites of deprotonation indicated by the superscripts in red. **b** Structure of kermesic acid, carminic acid and methoxatin with their sites of deprotonation indicated by the superscripts in red. **c** Structure of resveratrol and caulperinic acid with their sites of deprotonation indicated by the superscripts in red. **d** Structure of ommatin D and deoxysantalin with their sites of deprotonation indicated by the superscripts in red
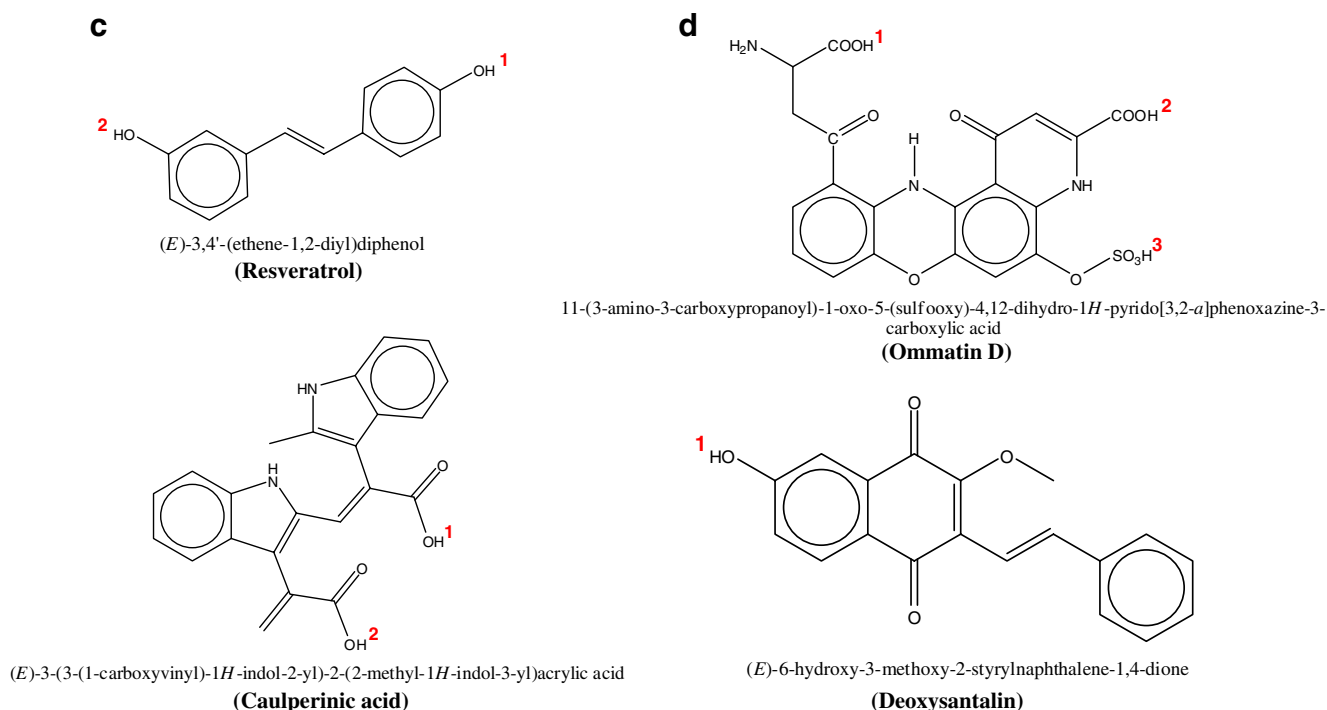
c

(E)-3,4'-(ethene-1,2-diyl)diphenol
(Resveratrol)

(E)-3-(3-(1-carboxyvinyl)-1H-indol-2-yl)-2-(2-methyl-1H-indol-3-yl)acrylic acid
(Caulperinic acid)

d

11-(3-amino-3-carboxypropanoyl)-1-oxo-5-(sulfooxy)-4,12-dihydro-1H-pyrido[3,2-a]phenoxazine-3-carboxylic acid
(Ommatin D)

(E)-6-hydroxy-3-methoxy-2-styrylnaphthalene-1,4-dione
(Deoxysantalin)

Fig. 1 (continued)

made after attempting with several high level calculations, as B3LYP showed convergence of wavelength maximum closer to the experimental values (within 10% deviation in most of the cases) than the other methods with minimum computational time. The theoretical evaluation of the electron density in the HOMO and LUMO of the dye molecules on photoexcitation has been carried out. The oxidation potentials, excitation energies and oscillator strengths at the optimized geometry in the ground state were determined using the time dependent DFT (TDDFT) calculations with the same basis set. The deprotonation order in terms of proton affinity (PA) has been evaluated at B3LYP/6-31G (d) level. The models of charge flow in the HOMO and LUMO have been visualized in Gauss view and presented. All calculations have been performed with the Gaussian 03 package [26].

Results and discussion

Ground state geometries and optical properties

It is important to have accurate information about the electronic structure of the natural pigments to gain insight into their photo induced electrochemical behaviour. The ground state geometries of the ten natural pigments selected for the present study were optimized in order to reveal their most probable electronic structure. The optimized stable

structures of the natural pigments were analyzed to assess the structural contribution of the molecule to its property. The first optically allowed electronic transitions of all the pigments are predicted to populate the 2^1A states (a HOMO → LUMO transition). The redox and other important characteristics of the pigments such as dominant configuration coefficient and oscillator strength have been evaluated by TDDFT and are summarized in Table 1. An important thermodynamic requirement of the dyes to be used in DSSC technology is that the HOMO level of the dye has to be sufficiently positive in the redox potential for efficient regeneration of the oxidized dye molecule to its original state by the hole conductor and the LUMO energy of the dye has to be sufficiently higher than the conduction band edge of the semiconductor (E_{CB}). The energies of HOMO and LUMO calculated for these natural pigments are given in Table 1. Importantly, the calculated excited state energies are all higher than the conduction band edge of TiO_2, the most widely used semiconductor for DSSC and hence, a thermodynamically favourable excited state electron injection from the dyes to TiO_2 is expected. The oxidation potential of HOMO and LUMO could be deduced by referencing the orbital energies (eV) to standardized electrode, NHE/SCE. This could be accomplished by shifting all predicted values by a common constant as is the general protocol for these comparisons [27, 28]. However as a direct method, the energy values of HOMO and LUMO levels of the dyes as compared with the band energies of TiO_2 [29] are illustrated

Table 1 Redox and spectral characteristics, dominant configuration coefficients (C) and oscillator strength (f) of natural pigments by TDDFT

Pigments	Energy (eV)		λmax (nm)		C	f
	HOMO	LUMO	Theoretical	Experimental		
Caffeic Acid	−6.29	−2.08	316	326 [30]	0.59	0.33
Ferulic Acid	−6.14	−2.02	317	307 [31]	0.62	0.43
Ellagic Acid	−6.49	−2.32	337	355 [32]	0.64	0.11
Kermesic acid	−6.39	−3.12	444	490 [33]	0.65	0.14
Carminic acid	−6.38	−3.13	444	495 [33]	0.65	0.17
Methoxatin	−7.26	−4.02	388	342 [34]	0.66	0.23
Resveratrol	−5.60	−1.65	333	326 [35]	0.63	0.87
Caulerpinic acid	−5.47	−2.14	435	309 [36]	0.64	0.19
Ommatin D	−5.73	−2.57	469	490 [37]	0.68	0.12
Deoxysantalin	−5.96	−3.28	543	*	0.63	0.16

*The experimental λmax is not available. The theoretical λmax (543 nm) is well within acceptable range, as deoxysantalin is reddish purple in colour and the reddish purple coloured solutions usually show their λmax in the range of 490 –545 nm.

in Fig. 2. From the excited state energies of these pigments, it can be inferred that all these pigments have sufficient driving force for electron injection to the conduction band of TiO$_2$. The theoretically predicted and experimentally observed wavelengths of maximum absorbance (λmax) of these pigments are given in Table 1. Close matching between the expected and theoretical λmax values has been observed for many of the molecules (within 10% deviation). Deviation in large molecules could be due to additional forces and steric strain that might prevail in their structures. In the case of methoxatin and caulerpinic acid, the deviations between theoretical and experimental λmax values are 46 nm and 126 nm respectively and their experimental values are blue-shifted. In the case of kermesic acid and carminic acid, the

deviations are 46 nm and 51 nm respectively and their λmax values are red-shifted. It is observed that molecules having hetero atoms with lone pair of electrons deviate the λmax values hypsochromically or bathochromically. If the hetero atom is a member of the ring and involved in conjugation it is observed to shift hypsochromically (methoxatin and caulerpinic acid) and if it is attached to the ring containing delocalized pi electron cloud, a bathochromic shift (kermesic acid and carminic acid) is observed. If the hetero atom does not contribute to the HOMO-LUMO transition (Ommatin D, Table 5), it does not affect the λmax value significantly. These discrepancies are generally due to charge transfer character of the corresponding transition. In particular, the blue shift occurs when the lone pair of electrons on the nitrogen atom

Fig. 2 HOMO (red colour) and LUMO (green colour) energies of photosensitizers compared with the band position of TiO2. (**a**) Caffeic acid (**b**) Ferulic acid (**c**) Ellagic acid (**d**) Kermesic acid (**e**) Carminic acid (**f**) Methoxatin (**g**) Resveratrol (**h**) Caulerpinic acid (**i**) Ommatin D (**j**) Deoxysantalin. The energy scale in electron volts referenced to the normal hydrogen electrode (NHE) or the vacuum level are also shown
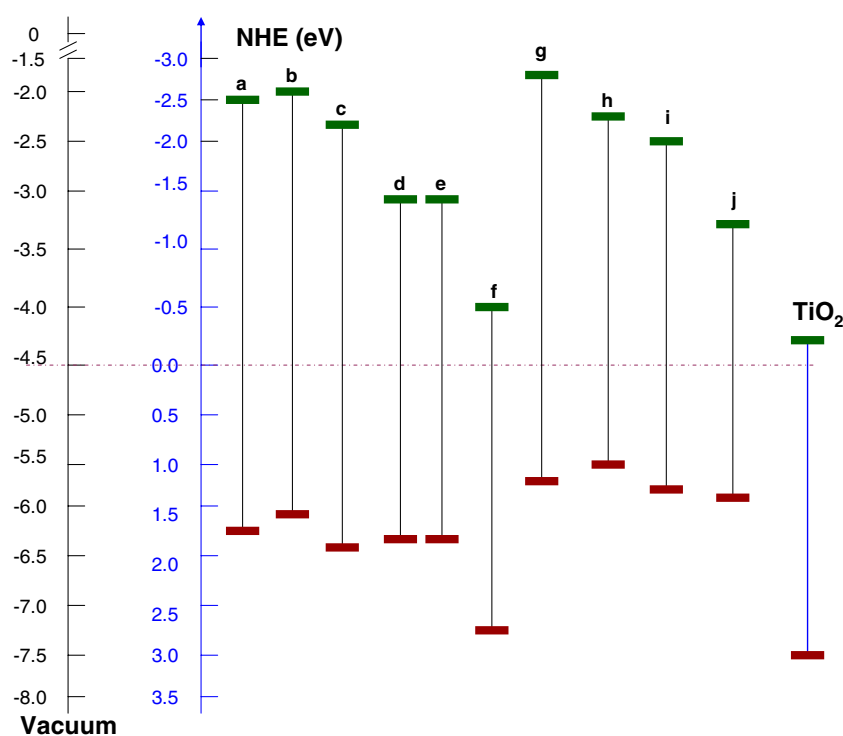
shows a diminished contribution to the conjugation due to charge transfer, ring strain and spatial orientation. The red shift could be attributed to the possibility of the keto-enol tautomeric form of the quinonoid rings during charge transfer, facilitating the auxochrome effect of the enolic group. TDDFT calculations provide dependable λ_{max} values for simple molecules. In large molecules with heteroatoms, TDDFT calculations coupled with flow visualization could lead to better understanding of the systems with tendency to deviate. The oscillator strength reflects the strength of transition from HOMO to LUMO and is used as a valuable tool for comparing transitions. The oscillator strength is high for resveratrol followed by ferulic acid, caffeic acid, methoxatin, carminic acid etc.

Generally, the configuration coefficients of interest are those which minimize the energy or belong to some selected eigen value [38]. In this study, the energy of the system, with interactions of the MOs involved in the dominant transition (HOMO and LUMO) has been considered for evaluating the configuration coefficient. It could be observed that the configuration coefficient of the dominant transitions of all the dyes studied, showed a value of ~0.60 and higher. The configuration coefficient of all other transitions was very low. It could be inferred that while a high configuration coefficient of the selected eigen values of the wave functions (HOMO and LUMO) could indicate the dominant transition, the usefulness of the pigments as photosensitizer is revealed by the high value of the oscillator strength.

Deprotonation orders

A requirement for the ideal dye structure in DSSCs is that it possesses several carbonyl or hydroxyl groups capable of chelating to the Ti (IV) sites on the titanium dioxide surface. Hence, we have examined the deprotonation order by comparing the energy difference between the optimized protonated and deprotonated structures (proton affinity, PA) [39]. As observed from Table 2, the proton affinity of the anchoring group varies from one molecule to the other and within the same molecule, from one structural environment to the other, bringing to the fore the strong dependence between the structure and the deprotonation order. The deprotonation order of the dyes reveals the most probable site of anchoring by the low values of PA. All the molecules studied are non-planar and hence spatial orientation and their environment could affect the deprotonation order. In the case of caffeic acid, the deprotonation order of hydrogen labelled 2 and 3 are almost similar and hence the anchoring to the semiconductor (TiO_2) can be expected at both these -OH groups. In the case of ferulic acid, anchoring at proton labelled 1 is favoured over that at 2 due to the low deprotonation energy (345.01 kcal mol^{-1}). In ellagic acid, all the protons are favourable for anchoring as they show similar deprotonation tendency. The proton labelled 2 in kermesic acid shows the anchoring tendency due to its low deprotonation energy, and also the feasibility for mononuclear bidentate coordination structure involving the flexible carbonyl group on the neighbouring carbon [40]. In carminic acid, the deprotonation sites labelled 5 and 6 show better anchoring property. In methoxatin, proton labelled 2 shows higher deprotonation tendency. In resveratrol the replaceable symmetrical protons show equal tendency for anchoring as revealed by their similar deprotonation order ~690.61 kcal mol^{-1}. In caulerpinic acid, the proton labelled 1 shows (373.91 kcal mol^{-1}) relatively better tendency for anchoring. In ommatin D protons of $-SO_3H$ (Labelled 3) has the lowest proton affinity and hence favourable for anchoring. In deoxysantalin, the only hydroxyl group proton shows efficient anchoring as revealed by charge flow in the HOMO and LUMO.

Table 2 Deprotonation order of the photosensitizers in terms of proton affinity (PA) by TDDFT

Photosensitizer	Deprotonation order (PA in Kcal/mol)								
	$(-H_1^+)$	$(-H_2^+)$	$(-H_3^+)$	$(-H_4^+)$	$(-H_5^+)$	$(-H_6^+)$	$(-H_7^+)$	$(-H_8^+)$	$(-H_9^+)$
Caffeic Acid	488.78	328.84	351.44	-	-	-	-	-	-
Ferulic Acid	345.01	420.32	-	-	-	-	-	-	-
Ellagic Acid	322.44	335.29	334.77	337.22	-	-	-	-	-
Kermesic acid	344.18	329.32	347.27	335.59	578.02	-	-	-	-
Carminic acid	380.78	371.54	341.75	516.79	325.03	309.95	353.07	366.11	374.71
Methoxatin	703.46	342.86	849.94	-	-	-	-	-	-
Resveratrol	690.61	690.62	-	-	-	-	-	-	-
Caulerpinic acid	373.91	912.24	-	-	-	-	-	-	-
Ommatin D	356.87	701.02	301.21	-	-	-	-	-	-
Deoxysantalin	682.08	-	-	-	-	-	-	-	-

HOMO-LUMO coupling and charge transfer

The HOMO and LUMO of all the pigments are given in Table 3, 4 and 5. In caffeic acid, both −OH groups on the benzyl ring are capable of providing good anchor to the semiconductor due to their predominant role in charge flow. This is also revealed by the high values of the bond length (0.9706 Å, 0.9701 Å) of the −OH bond (Table 6) as against the general equilibrium value of 0.956±0.015 Å. The −COOH group's contribution to the MOs is nil (Table 3). The delocalized pi electron cloud in benzene gets channeled towards the -COOH anchoring group (0.9707 Å) in ferulic acid. Under the influence of the high charge density on oxygen of −OH and −OCH₃ groups, the hydroxyl proton is not providing the anchor as also supported by HOMO and LUMO. Proton of the −COOH group with low PA could act as the anchor to the semiconductor. The extent of polarization of LUMO is very limited in ellagic acid due

to the higher symmetry of its HOMO. Charge distribution is more uniform and hence not highly favourable for injection of electron to the conduction band of the semi conductor as also evidenced by the oscillator strength (Table 1). The anthroquinone skeleton of kermesic acid favours the charge flow to the three −OH groups directly attached to the benzyl ring. Charge flow is more favoured towards −OH group with proton labelled 2. Correlation between PA and the charge flow characteristics in MOs indicate proton labelled 2 as the anchor group. Though LUMO has distinct polarized overlap of molecular orbitals of the −OH groups and the benzyl ring (Table 4) there is higher charge density in the molecule than towards the anchor which is also revealed by the oscillator strength. In carminic acid, the absence of unsaturation in the ring containing the protons labelled 1, 2, 8 and 9 eliminate these for anchoring. Due to the intramolecular H- bonding between the −OH groups labeled 5 and 6, charge flow is

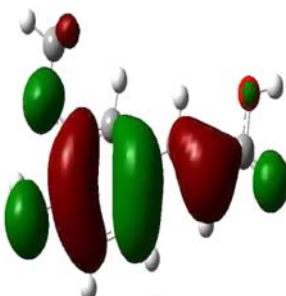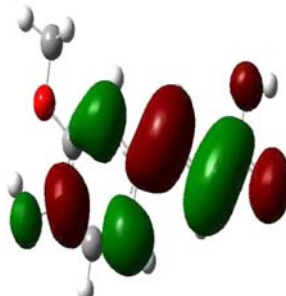**Table 3** HOMO and LUMO of caffeic acid, ferulic acid and ellagic acid
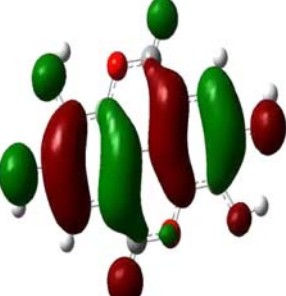
Pigment	HOMO	LUMO
Caffeic acid		
Ferulic acid		
Ellagic acid		

Table 4 HOMO and LUMO of kermesic acid, carminic, methoxatin and resveratrol
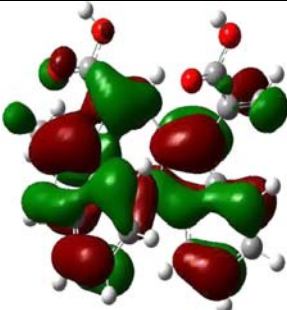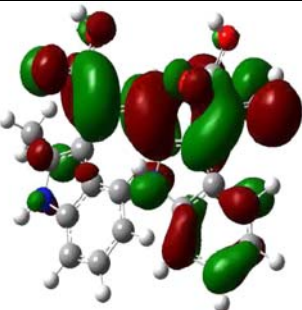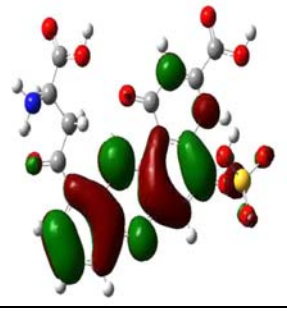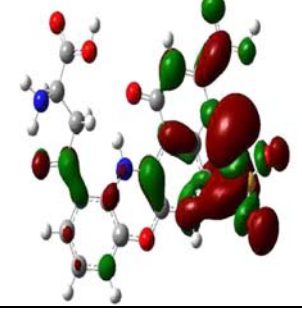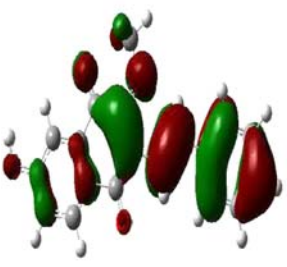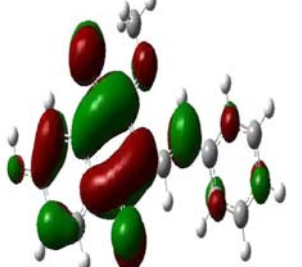
Pigment	HOMO	LUMO
Kermesic acid		
Carminic acid		
Methoxatin		
Resveratrol		

restricted (Fig. 1b). Similar electron density around −OH (5 and 6) protons both in HOMO and LUMO indicates the presence of a stabilizing force which could be attributed to the hydrogen bonding. Similarly the H-bond between 5th and 7th OH group protons each with the adjacent carbonyl group is also probable as revealed by near equal electron density present in HOMO and LUMO caused by such stabilization. Hence protons labelled 3 and 4 are involved in anchoring as supported by the charge flow patterns. Proton 3 is more favoured for anchoring by its low PA.

Strong coupling between the pi electrons of the pyridyl ring and the two −COOH groups with protons labelled 1 and 3, makes the electron cloud delocalization to the anchoring group less feasible in methoxatin. Proton with label 2 is a relatively better anchor with its low PA (342.86 kcal mol^{-1}). Migration of electron cloud towards

Table 5 HOMO and LUMO of caulperinic acid, ommatin D and deoxysantalin

Pigment	HOMO	LUMO
Caulperinic acid		
Ommatin D		
Deoxysantalin		

the anchoring group is very strong and well mediated by the bridging configuration in the case of reservatrol (Table 4). In the case of caulerpinic acid, the migratory aptitude of the electron density in heteronuclear ring is good but it results in the strong coupling between the methylene group and −COOH group leading to a weak deprotonation of proton labelled 2. Charge flow in LUMO towards carboxyl proton 1 is evident from Table 5 and also supported by the low PA. In Ommatin, the absence of extended conjugation eliminates the anchoring through the proton labelled 1. Proton 2 is well stabilized by the pyrido ring making proton 3 the favourable site of anchoring. This is evident from the charge flow pattern in the LUMO. However, the oscillator strength is low in ommatin D due to the coupling between −O-SO$_3$H and −NH- groups and hence the electron density does not rest on the anchoring group (Table 5). In deoxysantalin the delocalization of the electron cloud centered on the benzoquinone moiety is only

partial as it contributes to both HOMO and LUMO. This suppresses the effective charge transfer.

The bond length of the anchor groups has been evaluated for the optimized geometry of the ten photosensitizers (Table 6). Correlation of the charge flow, PA and the bond lengths reveal that the −OH groups are the better anchoring groups in the photosensitizers studied than −COOH, under otherwise similar structural environment. This is because binding *via* the hydroxyl group results in a very strong chromophore-semiconductor coupling as only a single oxygen atom separates the chromophores from the semi-conductor. The chromophore-semiconductor coupling decreases with carboxyl binding when compared to hydroxyl groups [41]. In all the natural pigments studied, the bond length of the anchoring

−OH proton has been observed to be about 0.971 Å, but other non-anchoring -OH protons also showed this value of (about 0.971 Å) bond length. Hence it could be indicated

Table 6 Optimized bond length of the anchoring groups of the photosensitizers

Photosensitizer	Label of replaceable proton and its bond length (Å)				
	1	2	3	4	5
Caffeic acid	−COOH 0.9723	−OH 0.9706	−OH 0.9701	-	-
Ferulic acid	−COOH 0.9707	−OH 0.9710	-	-	-
Ellagic acid	−OH 0.9701	−OH 0.9715	−OH 0.9709	−OH 0.9719	-
Kermesic acid	−OH 0.9674	−OH 0.9666	−OH 0.9710	−COOH 0.9702	−OH 0.9691
Methoxatin	−COOH 0.9705	−COOH 0.9704	−COOH 0.9708	-	-
Resveratrol	−OH 0.9710	−OH 0.9711	-	-	-
Caulerpinic acid	−COOH 0.9707	−COOH 0.9707	-	-	-
Ommatin D	−COOH 0.9711	−COOH 0.9703	−OSO$_3$H 0.9399	-	-
Deoxysantalin	−OH 0.9709	-	-	-	-
Carminic acid[+]	−OH 0.9600	−OH 0.9618	−OH 0.9707	−COOH 0.9708	−OH 0.9709
	6[+] −OH 0.9709	7[+] −OH 0.9702	8[+] −OH 0.9654	9[+] −OH 0.9597	-

[+] Replaceable protons labelled 6–9 on Carminic acid are appended.

that −OH bond length of about 0.971 Å associated with the low PA value could form the anchoring group in the dye molecule. As observed from Tables 3, 4 and 5, there is clear shift in the electron density in the frontier molecular orbitals (MOs) during HOMO → LUMO photoexcitation from the core of the molecule to the anchoring group in all pigments studied. Such movement of electron distribution will favour electron injection from the dye to semiconductor.

Conclusions

The ground state geometries, electronic structures, photo-electrochemical redox characteristics, deprotonation energies, bond length of anchoring groups and the charge flow between the HOMO- LUMO of the ten natural dye pigments have been evaluated by TDDFT calculations. The results show that the dominant electronic transitions populate the 2^1A state (a HOMO → LUMO transition). The electron distribution before the light irradiation locates mainly on the donor units; whereas after light irradiation it moves to the acceptor units close to the anchoring groups, which favours the electron injection from the dye molecules to the conduction band edge of TiO$_2$. The ground state oxidation potentials and the excited state oxidation potentials reveal that the electron transfer from the dye molecules

to the TiO$_2$ conduction band is thermodynamically favourable in all the pigments studied. This study highlights that the −OH group attached to the ring of delocalized π electron cloud acts as the best anchor. The flexible spatial orientation provided by the ethylene bridge to the light absorbing moiety as in the case of reservatrol is the additional favoured feature. Based on HOMO-LUMO coupling and the oscillator strength reservatrol emerges as the potential photosensitizer for application in DSSC. Also ferulic acid, caffeic acid and methoxatin find theoretical merit to be used as photosensitizers. A recent study [42] on dye sensitized solar cell using carminic acid as the photosensitizer has reported an open circuit voltage (V$_{oc}$) of 0.34 V and short circuit current (I$_{sc}$) of 390 μA. Our theoretical study has brought to light the other potential photosensitizers also such as resveratrol, ferulic acid, caffeic acid and methoxatin for efficient application in DSSC due to their favourable wavelength maximum much compatible with TiO$_2$ and their high oscillator strength. If the oscillator strength is high, then the electron excitation is highly favoured and hence such molecules could efficiently play the role of the photosensitizer.

References

1. Nazeeruddin MK, Kay A, Rodico J, Humphry Baker R, Muller E, Liska P, Vlachopoulos N, Gratzel M (1993) Conversion of light to electricity by cis-X2bis (2, 2′- bipyridyl-4, 4′-dicarboxylate) ruthenium (II) charge-transfer sensitizers (X = Cl-, Br-, I-, CN- and SCN-) on nanocrystalline titanium dioxide electrodes. J Am Chem Soc 115:6382–6390. doi:10.1021/ja00067a063

2. Smestad G, Bignozzi C, Argazzi A (1994) Testing of dye sensitized TiO_2 solar cells I: Experimental photocurrent output and conversion efficiencies. Sol Energy Mater Sol Cells 32:259–272. doi:10.1016/0927-0248(94)90263-1

3. Nazeeruddin MK, Pechy P, Gratzel M (1997) Efficient panchromatic sensitization of nanocrystalline TiO_2 films by a black dye based on a trithiocyanato-ruthenium complex. J Chem Commun 1705-1706. doi:10.1039/a703277c

4. Grätzel M (2003) Dye-sensitized solar cells. J Photochem Photobiol C: Photochem Rev 4:145–153. doi:10.1016/S1389-5567(03)00026-1

5. Runge E, Gross EKU (1984) Density-Functional Theory for Time-Dependent Systems. Phys Rev Lett 52:997–1000. doi:10.1103/PhysRevLett.52.997

6. Jacquemin D, Perpète EA, Ciofini I, Adamo C (2008) On the TD-DFT UV/vis spectra accuracy: the azoalkanes. Theor Chem Account 120:405–410. doi:10.1007/s00214-008-0424-9

7. Hao S, Wu J, Huang Y, Lin J (2006) Natural dyes as photosensitizers for dye-sensitized solar cell. Sol Energy 80:209–214. doi:10.1016/j.solener.2005.05.009

8. Polo AS, Iha NY (2006) Blue sensitizers for solar cells: Natural dyes from Calafate and Jaboticaba. Sol Energy Mater Sol Cells 90:1936–1944. doi:10.1016/j.solmat.2006.02.006

9. Garcia CG, Polo AS, Iha NY (2003) Fruit extracts and ruthenium polypyridinic dyes for sensitization of TiO_2 in photo electrochemical solar cells. J Photochem Photobiol A 160:87–91. doi:10.1016/S1010-6030(03)00225-9

10. Smestad GP (1998) Education and solar conversion: Demonstrating electron transfer. Sol Energy Mater Sol Cells 55:157–178. doi:10.1016/S0927-0248(98)00056-7

11. Olea A, Ponce G, Sebastian PJ (1999) Electron transfer via organic dyes for solar conversion. Solar Energy Mater Sol Cells 59:137–143. doi:10.1016/S0927-0248(99)00038-0

12. Cherpy NJ, Smestad GP, Gratzel M, Zhang JZ (1997) Ultrafast Electron Injection: Implications for a Photoelectrochemical Cell Utilizing an Anthocyanin Dye- Sensitized TiO_2 Nanocrystalline Electrode. J Phys Chem B 101:9342–9351. doi:10.1021/jp972197w

13. Kumara GRA, Kanebo S, Okuya M, Onwona-Agyeman B, Konno A, Tennakone K (2006) Shiso leaf pigments for dye-sensitized solid-state solar cell. Solar Energy Mater Sol Cells 90:1220–1226. doi:10.1016/j.solmat.2005.07.007

14. Garcia CG, Polo AS, Murakami Iha NY (2003) Photoelectrochemical solar cell using extract of Eugenia jambolana Lam as natural sensitizer. An Acad Bras Cienc 75:163–165

15. Tennakone K, Kumarasinghe AR, Kumara GRRA, Wijayantha KGU, Sirimanne M (1997) Nanoporous TiO_2 photo anode sensitized with the flower pigment cyaniding. J Photochem Photobiol A: Chem 108:193–195. doi:10.1016/S1010-6030(97)00090-7

16. Hedbor S, Klar L (2005) Plant Extract Sensitised Nanoporous Titanium Dioxide Thin Film Photoelectrochemical Cells. Dissertation, Uppsala University

17. Yamazaki E, Murayama M, Nishikawa N, Hashimoto N, Shoyama M, Kurita O (2007) Utilization of natural carotenoids as photosensitizers for dye-sensitized solar cells. Sol Energy 81:512–516. doi:10.1016/j.solener.2006.08.003

18. Wongcharee K, Meeyoo V, Chavadej S (2007) Dye-sensitized solar cell using natural dyes extracted from rosella and blue pea flowers. Solar Energy Mater Sol Cells 91:566–571. doi:10.1016/j.solmat.2006.11.005

19. Starck D, Vogt T, Schliemann W (2003) Recent advances in betalain research. Phytochem 62:247–269. doi:10.1016/S0031-9422(02)00564-2

20. Lai WH, Su YS, Teoh LG, Hon MH (2007) Commercial and natural dyes as photosensitizers for a water-based dye-sensitized solar cell loaded with gold nanoparticles. J Photochem Photobiol A: Chem 195:307–313. doi:10.1016/j.jphotochem.2007.10.018

21. Calogero G, Marco GD (2008) Red Sicilian orange and purple eggplant fruits as natural sensitizers for dye-sensitized solar cells. Solar Energy Mater Sol Cells 92:1341–1346. doi:10.1016/j.solmat.2008.05.007

22. Lee C, Yang W, Parr RG (1988) Development of the Colle-Salvetti Correlation-Energy Formula into a Functional of the Electron Density. Phys Rev B 37:785–789. doi:10.1103/PhysRevB.37.785

23. Becke AD (1993) Density-functional thermochemistry. III. The role of exact exchange. J Chem Phys 98:5648–5652. doi:10.1063/1.464913

24. Ditchfield R, Hehre WJ, Pople JA (1971) Self-Consistent Molecular-Orbital Methods. IX. An Extended Gaussian-Type Basis for Molecular-Orbital Studies of Organic Molecules. J Chem Phys 54:724–728. doi:10.1063/1.1674902

25. Carlos Bustos C, Christian Sánchez C, Rolando Martínez R, Ricardo Ugarte R, Eduardo Schott E, Carey DML, Garland MT, Espinoza L (2007) Tautomeric, spectroscopic, DFT calculations and ray studies on O2N-4-C6H4-NHN-C(COCH3)2. Dyes and Pigments 74:615–621. doi:10.1016/j.dyepig.2006.04.002

26. Frisch MJ, Trucks GW, Schlegel HB, Scuseria GE, Robb MA, Cheeseman JR, Montgomery Jr. JA, Vreven T, Kudin KN, Burant, JC, Millam JM, Iyengar SS, Tomasi J, Barone V, Mennucci B, Cossi M, Scalmani G, Rega N, Petersson GA, Nakatsuji H, Hada M, Ehara M, Toyota K, Fukuda R, Hasegawa J, Ishida M, Nakajima T, Honda Y, Kitao O, Nakai H, Klene M, Li X, Knox JE, Hratchian HP, Cross JB, Bakken V, Adamo C, Jaramillo J, Gomperts R, Stratmann RE, Yazyev O, Austin AJ, Cammi R, Pomelli C, Ochterski JW, Ayala PY, Morokuma K, Voth GA, Salvador P, Dannenberg JJ, Zakrzewski VG, Dapprich S, Daniels AD, Strain MC, Farkas O, Malick DK, Rabuck AD, Raghavachari K, Foresman JB, Ortiz, JV, Cui Q, Baboul AG, Clifford S, Cioslowski J, Stefanov BB, Liu G, Liashenko A, Piskorz P, Komaromi I, Martin RL, Fox DJ, Keith T, Al-Laham MA, eng CY, Nanayakkara A, Challacombe M, Gill PMW, Johnson B, Chen W, Wong MW, Gonzalez C, Pople JA (2003) Gaussian 03, Gaussian Inc, Pittsburgh, PA

27. Reiss H, Heller A (1985) The absolute potential of the standard hydrogen electrode: a new estimate. J Phys Chem 89:4207–4213. doi:10.1021/j100266a013

28. Cossi M, Iozzi MF, Marrani AG, Lavecchia T, Galloni P, Zanoni R, Decker F (2006) Measurement and DFT Calculation of Fe(cp) 2 Redox Potential in Molecular Monolayers Covalently Bound to H-Si(100). J Phys Chem B 110:22961–22965. doi:10.1021/jp064800t

29. Grätzel M (2001) Photoelectrochemical cells. Nature 414:338–344

30. Harborne JB, Harborne AJ (1998) Phytochemical methods: a guide to modern techniques of plant analysis, 3rd edn. Springer, Berlin, pp. 53–54

31. Lin FH, Lin JY, Gupta RD, Tournas JA, Burch JA, Selim MA, Monteiro-Riviere NA, Grichnik JM, Zielinski J, Pinnell SR (2005) Ferulic Acid Stabilizes a Solution of Vitamins C and E and Doubles its Photoprotection of Skin. J Investigative Dermatol 125:826–832. doi:10.1111/j.0022-202X.2005.23768.x

32. Dixit R, Gold B (1986) Inhibition of N-methyl-N-nitrosourea-induced mutagenicity and DNA methylation by ellagic acid. Proc Natl Acad Sci 83:8039–8043

33. Balakina GG, Vasiliev VG, Karpova EV, Mamatyuk VI (2006) HPLC and molecular spectroscopic investigations of the red dye

obtained from an ancient Pazyryk textile. Dyes and Pigments 71:54–60. doi:10.1016/j.dyepig.2005.06.014

34. Robertson JG, Alok Kumar J, Mancewicz UA, Villafranca JJ (1989) Spectral Studies of Bovine Dopamine, & Hydroxylase. J Biol Chem 264:19916–19921

35. Polunin KE, Sokolova NP, Gorbunov AM, Bulgakova RA, Polunina IA (2007) FTIR Spectroscopic Studies of Interactions of Stilbenes with Silicon Dioxide. Protection of Metals 44:352–357

36. Anjaneyulu ASR, Prakash CVS, Mallavadhani UV (1991) Two Caulerpin analogues and a sesquiterpene from caulerparacemosa. Phytochem 30:3041–3042

37. Martel RR, Laws JH (1991) Purification and Propertieso f an Ommochrome-binding Protein from the Hemolymph of the Tobacco Hornworm, Manduca sexta. J Biol Chem 266:21392–21396

38. Ba´lint I, Dezso G, Gyemant I (2000) A perfectly N-representable two-particle density matrix for the electron correlation problem.

THEOCHEM 501–502:125–131. doi:10.1016/S0166-1280(99)00421-2

39. Qin C, Clark AE (2007) DFT characterization of the optical and redox properties of natural pigments relevant to dye-sensitized solar cells. Chem Phys Lett 438:26–30. doi:10.1016/j.cplett.2007.02.063

40. Liu Z (2008) Theoretical studies of natural pigments relevant to dye-sensitized solar cells. THEOCHEM 862:44–48. doi:10.1016/j.theochem.2008.04.022

41. Duncan WR, Prezhdo OV (2006) Theoretical Studies of Photoinduced Electron Transfer in Dye-Sensitized TiO_2. Ann Rev Phys Chem 58:143–184. doi:10.1146/annurev.physchem.58.052306.144054

42. Padova PD, Lucci M, Olivieri B, Quaresima C, Priori S, Francini R, Grilli A, Hricovini K, Davoli I (2009) Natural hybrid organic_inorganic photovoltaic devices. Superlattices and Microstructures 45:555–563. doi:10.1016/j.spmi.2009.03.005